Philosophical Magazine Letters,
Vol. 86, No. 2, February 2006, 99–112

Taylor & Francis
Taylor & Francis Group

Two-dimensional viscoelastic discrete triangular system with negative-stiffness components

Y.-C. WANG*†, J. G. SWADENER† and R. S. LAKES‡

†Materials Science and Technology Division, MST-CINT, Los Alamos National Laboratory, Los Alamos, NM 87545, USA
‡Department of Engineering Physics, Engineering Mechanics Program, Biomedical Engineering Department, Materials Science Program and Rheology Research Center, University of Wisconsin–Madison, 147 Engineering Research Building, 1500 Engineering Drive, Madison, WI 53706-1687, USA

(*Received 22 September 2005; in final form 3 January 2006*)

Potential applications of high-damping and high-stiffness composites have motivated extensive research on the effects of negative-stiffness inclusions on the overall properties of composites. Recent theoretical advances have been based on the Hashin–Shtrikman composite models, one-dimensional discrete viscoelastic systems and a two-dimensional nested triangular viscoelastic network. In this paper, we further analyze the two-dimensional triangular structure containing pre-selected negative-stiffness components to study its underlying deformation mechanisms and stability. Major new findings are structure-deformation evolution with respect to the magnitude of negative stiffness under shear loading and the phenomena related to dissipation-induced destabilization and inertia-induced stabilization, according to Lyapunov stability analysis. The evolution shows strong correlations between stiffness anomalies and deformation modes. Our stability results reveal that stable damping peaks, i.e. stably extreme effective damping properties, are achievable under hydrostatic loading when the inertia is greater than a critical value. Moreover, destabilization induced by elemental damping is observed with the critical inertia. Regardless of elemental damping, when the inertia is less than the critical value, a weaker system instability is identified.

1. Introduction

In recent years, negative-stiffness-induced effective stiffness and damping anomalies have been quite extensively studied, experimentally [1, 2] and theoretically [3, 4]. In the realm of mathematical modelling of a physical process, the behavior of the model in space, time and material (or system-specific) parameter spaces are of particular interest. Recognition that inclusions have negative stiffness has added another degree of freedom in the design of composite materials. In structural mechanics, negative stiffness is obtainable through post-buckling processes. In solid materials, the Landau phenomenological theory of phase transformations predicts negative curvature in the system free-energy, i.e. a negative stiffness in the vicinity of phase transitions.

*Corresponding author. Email: yunche@lanl.gov

Philosophical Magazine Letters
ISSN 0950-0839 print/ISSN 1362-3036 online © 2006 Taylor & Francis
http://www.tandf.co.uk/journals
DOI: 10.1080/09500830600567719

For discrete viscoelastic systems with negative-stiffness components, our previous studies have shown that the stability of the most interesting configuration that corresponds to extreme overall stiffness is metastable, both in one- and two-dimensional systems [5, 6]. Singularly stable extreme damping has been theoretically shown in one dimension [7]. In general, metastability entails that an energy minimizer of a system does not exist. Observation of metastability is possible and has been reported in other studies, such as liquid droplets on hydrophilic or hydrophobic surfaces [8]. In the negative-stiffness systems, the degree of metastability for discrete negative-stiffness composite systems may be tuned *via* the viscoelastic properties of each composing element. In contrast, isotropic and homogeneous negative-Poisson's ratio ($-1 < \nu < 0$) materials are stable, both in theory and experimentally [9, 10]. Furthermore, for an isotropic and homogeneous continuum, it is well known that uniqueness of linear elasticity solutions is ensured if strong ellipticity criteria are satisfied [11, 12]. Violation of strong ellipticity causes band formation in deformation processes; hence instability occurs. Stability, in the sense of energy minimization, of a continuum with negative stiffness under different loading conditions has been studied and summarized in [13].

The stability of a discrete negative-stiffness composite system is intriguing. A negative-stiffness system stabilized by follower forces (forces whose direction changes in accord with the system's deformation) has been demonstrated by Thompson [14]. The destabilization paradox [15] states that the stability of certain non-conservative systems is weaker due to dissipation. Yet, it is well known that dissipation can help stabilize or destabilize a system. Gyroscopic systems with a definite-negative stiffness matrix can be stabilized by certain damping mechanisms [16]. An unconstrained negative-stiffness object in a conservative system is unstable. However, to some degree, it can be stabilized in the form of composites with a positive-stiffness surrounding matrix, as studied in one-dimensional [5, 17, 18] and two-dimensional [6] systems. The latter is a pre-cursor of our present study. In [6], the structural evolution of a nested triangular lattice cell with respect to negative stiffness assigned to pre-selected components under hydrostatic loading is studied in detail. With pre-chosen inertia in the system, the results of stability analysis in that work identify a system-related instability with an amount of negative stiffness less than that required for singularly stable damping peak, contrary to experience from one-dimensional systems.

In this paper, we study in particular the structural evolution of the triangular system with negative stiffness under shear. Our Lyapunov stability analysis with different inertia and elemental damping reveals the phenomena of dissipation-induced destabilization and inertia-induced stabilization in the system under the influences of negative stiffness. We show that stable extreme effective damping in two dimensions is achievable.

2. Analysis

To analyze the nested triangular structure, as shown in figure 1, with the components of the inner triangle containing negative stiffness (i.e. $k_1 < 0$), and $k_2 = 5$ and

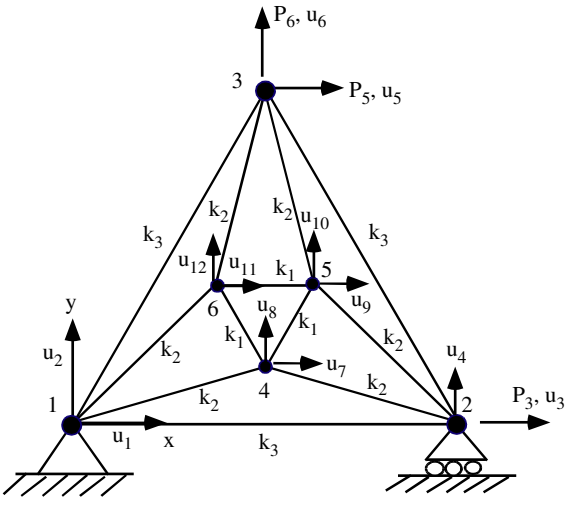

Figure 1. The nested triangular lattice cell. Solid circles denote the j-th nodal mass, M_j. We assume that M_j is the same for all j throughout the analysis. The inner triangle consists of the standard linear solid component with the spring constant k_1, the outer triangle with k_3 and the linking components between the inner and outer triangle with k_2. Viscoelastic time constants for the components are fixed and given in section 3.1. The spring constant k_1 is to be tuned negative to observe stiffness and damping anomalies along the loading direction for a given loading condition. The length of the inner triangle is 5 mm and that of outer triangle 28 mm; both triangles share the same centre. We denote u_m and P_m for the displacement and loading, respectively, for the m-th degree of freedom.

$k_3 = 10\,\mathrm{kN/m}$ being fixed throughout, we adopt the finite-element method (FEM) for its simplicity and efficiency in handling systems with many degrees of freedom [19, 20]. Detailed matrices used in the FEM calculations can be found in [6]. Here, we present the framework of our analysis; particular attention is placed on the FEM in terms of the state-space presentation. All the numerical calculations here were performed with the software Mathematica 5.0® (Wolfram Research, Inc., Champaign, IL, USA).

2.1. *Equations of motion and loading conditions*

According to Newton's second law, the equations of motion at each node along the x and y directions can be expressed in matrix form as follows:

$$\boldsymbol{M} \bullet \ddot{\boldsymbol{U}} + \boldsymbol{F} = \boldsymbol{P} \tag{1}$$

$$\boldsymbol{F} = \boldsymbol{\Lambda}^T \bullet \boldsymbol{f} \tag{2}$$

Here, $\boldsymbol{U}$ is the displacement vector, $\boldsymbol{M}$ the lumped-mass matrix, $\boldsymbol{P}$ the external force vector and $\boldsymbol{F}$ the internal force vector, which is computed from the internal force $\boldsymbol{f}$ in the element's local coordinates. Uppercase letters are designated to indicate variables in the global coordinates. The symbol $\boldsymbol{\Lambda}$ denotes a transformation matrix

between the global and local coordinates [6]. The symbol • represents the inner product between matrix and vector, or among matrices. A super dot indicates differentiation with respect to time, two super dots indicate the second time derivative, and the superscript T denotes the transpose operation of a matrix. The relationship between $\boldsymbol{U}$ and $\boldsymbol{f}$ requires a constitutive law, discussed in section 2.2.

We prescribe pre-chosen loading conditions to study the effective bulk stiffness (K_b), shear stiffness (K_s) and compressive stiffness (K_c) in a range of k_1, including negative values. Applying hydrostatic compression,

$$P_3 = -p\cos\left(\frac{\pi}{6}\right), \quad P_5 = 0, \quad P_6 = -p \tag{3}$$

we calculate the effective bulk stiffness (K_b) through the equation, $K_b = P_6/u_6$. Assigning

$$P_3 = -\frac{p}{2}, \quad P_5 = p, \quad P_6 = 0 \tag{4}$$

the shear stiffness is calculated by $K_s = P_5/u_5$. Under the uni-axial compression,

$$P_3 = 0, \quad P_5 = 0, \quad P_6 = -p \tag{5}$$

the equation $K_c = P_6/u_6$ gives rise to the effective compressive stiffness. Here, we use the convention that assumes the loading parameter $p > 0$ is compressive.

2.2. *Constitutive relations*

The standard linear solid model [21] is adopted in our present analysis since it has a sufficiently general frequency response to represent viscoelastic materials for the present purposes.

$$f_j + T_{\varepsilon j}\dot{f}_j = k_j\left(\Delta_j + T_{\sigma j}\dot{\Delta}_j\right), \quad j = 1, 2, \ldots, n \tag{6}$$

Here n is the number of elements. f_j and Δ_j represent the internal force and change of length of the element j, respectively. Note that $T_{\varepsilon j}$ and $T_{\varepsilon j}$ are in units of time, and the loss tangent of the j-th element is $\tan\delta_j = ((\omega(T_{\sigma j} - T_{\varepsilon j}))/(1 + \omega^2 T_{\sigma j} T_{\varepsilon j}))$ at the frequency ω. When $T_{\varepsilon j} = T_{\sigma j} = 0$ for all j, this model reduces to Hooke's law. We further define

$$r = \frac{T_{\sigma j}}{T_{\varepsilon j}}, \quad \text{for all } j \tag{7}$$

to indicate the relaxation strength for all the components. Here, we assume a constant r, but different $T_{\sigma j}$ and $T_{\varepsilon j}$ (given in section 3.1) for different j throughout analysis. In other words, initially, the k_1, k_2 and k_3 standard linear solid components have pre-chosen but different viscoelastic time constants. During a numerical scan in the r parameter space, elemental damping properties of all the components increase or decrease by the same magnitude, r. A graph delineating the relationship between r and loss tangent with a given $T_{\varepsilon j}$ under different frequency is given in [6].

2.3. *State–space representation*

Combining the equations of motion and the constitutive relation, equations (1), and (6), the mechanical system can be modelled in terms of the state–space variables (X), as follows. Let subscript m be the number of degrees of freedom.

$$\boldsymbol{A} \bullet \dot{\boldsymbol{X}} = \boldsymbol{B} \bullet \boldsymbol{X} + \boldsymbol{C} \tag{8}$$

$$\boldsymbol{A} = \begin{bmatrix} \boldsymbol{I}_m & \boldsymbol{0} & \boldsymbol{0} \\ \boldsymbol{0} & \boldsymbol{M} & \boldsymbol{0} \\ \boldsymbol{0} & \boldsymbol{0} & \boldsymbol{T}_\varepsilon \end{bmatrix} \tag{9}$$

$$\boldsymbol{B} = \begin{bmatrix} \boldsymbol{0} & \boldsymbol{I}_m & \boldsymbol{0} \\ \boldsymbol{0} & \boldsymbol{0} & -\boldsymbol{\Lambda}^T \\ \boldsymbol{k}_{\text{ele}} \bullet \boldsymbol{\Lambda} & \boldsymbol{k}_{\text{ele}} \bullet \boldsymbol{T}_\sigma \bullet \boldsymbol{\Lambda} & -\boldsymbol{I}_n \end{bmatrix} \tag{10}$$

$$\boldsymbol{C} = [\,\boldsymbol{0} \quad \boldsymbol{P}^T \quad \boldsymbol{0}\,]^T \tag{11}$$

The state–space variables are $\boldsymbol{X} = [\,\boldsymbol{U} \quad \boldsymbol{V} \quad \boldsymbol{f}\,]^T$, where $\boldsymbol{U}$ is the displacement vector, $\boldsymbol{V}$ the velocity vector and $\boldsymbol{f}$ the vector containing internal force for all the elements. $\boldsymbol{I}$ is a square identity matrix with the dimension m by m, and $\boldsymbol{k}_{\text{ele}}$ represents the stiffness matrix in the local coordinate system. $\boldsymbol{T}_\sigma$ and $\boldsymbol{T}_\varepsilon$ are matrices containing the viscoelastic time constants for each element. The matrices, $\boldsymbol{k}_{\text{ele}}$, $\boldsymbol{T}_\sigma$ and $\boldsymbol{T}_\varepsilon$, are diagonal, as is the matrix $\boldsymbol{M}$. The j-th component of $\boldsymbol{M}$ is denoted by M_j for node j. In later numerical calculations, we assume M_j is the same for any j. Explicit expressions of these matrices can be found in [6]. We use the symbol λ_k for the k-th mode in the state space to denote the eigenvalue of the matrix $\boldsymbol{A}^{-1} \bullet \boldsymbol{B}$ in the Lyapunov stability analysis.

2.4. *Linear viscoelastic damping and stability*

Effective damping and stability depend on the viscosity of each element and driving frequency (ω). To calculate the damping properties of the system in terms of the loss tangent, we take a Fourier transformation on the governing equations, equations (1), (2) and (6), to obtain the dynamic (or complex) stiffness of the system in the frequency domain, as follows.

$$\boldsymbol{K}^* = -\omega^2 \boldsymbol{M} + \boldsymbol{\Lambda}^T \bullet (\boldsymbol{I}_n + i\omega \boldsymbol{T}_\varepsilon)^{-1} \bullet (\boldsymbol{k}_{\text{ele}} \boldsymbol{\Lambda} + i\omega \boldsymbol{k}_{\text{ele}} \boldsymbol{T}_\sigma \boldsymbol{\Lambda}). \tag{12}$$

By the generalization of the definition of the loss tangent for a 1-DOF system, the effective loss tangent of the system can be calculated as follows:

$$\tan \delta_j = \frac{\text{Im}(\zeta_i)}{\text{Re}(\zeta_j)}, \quad j = 1, 2, \ldots, n. \tag{13}$$

Here ζ_j is the eigenvalue of $\boldsymbol{K}^*$, providing phase information for the deformation mode j. In other words, each of the loss-tangent components corresponds to the phase lag information of a specific load-deformation mode. Notice that the

eigenvalues ζ_j and λ_k are fundamentally different. The former are the eigenvalues of the complex stiffness matrix and the latter are the stability eigenvalues used in the Lyapunov stability analysis.

According to the Lyapunov indirect theorem, the stability of the dynamical system, equations (8)–(11), may be determined by simply investigating the eigenvalues (λ_k) of the matrix $\mathbf{A}^{-1} \bullet \boldsymbol{B}$. The imaginary part of λ_k provides the oscillatory information for the normal mode k in the state space, whereas the real part of λ_k determines the stability of the system. If $\mathrm{Re}(\lambda_k) > 0$, the system is unstable; otherwise, the system is stable. Here, we look for eigenvalues with their real parts greater than zero while tuning the amount of negative stiffness in the pre-chosen elements (i.e. the k_1 elements). We remark that Lyapunov's indirect theorem predicts only local stability – consistent with our linear analysis.

3. Results and discussion

In the present analysis, the spring constants $k_2 = 5$ and $k_3 = 10\,\mathrm{kN/m}$ are unchanged throughout. The absolute values of k_2 and k_3 are irrelevant to the search of the anomalies in the overall viscoelastic responses of the system when tuning k_1, since only the ratios between them are significant.

3.1. *Effective stiffness and damping anomalies*

Figure 2 shows the anomalous peaks and anti-peaks in the effective stiffness for K_b, K_c and K_s arising from the negative-stiffness effects from the inner triangle. Between each peak and anti-peak pair for all the loading conditions, the effective stiffness is negative, which is unstable, according to the energy argument. Elsewhere the effective stiffness is positive. The system stability boundaries 1 and 2 are determined *via* Lyapunov stability analysis with inertia $M_j \leq 10^{-12}$ and $M_j \geq 10^{-6}\,\mathrm{kg}$, respectively, and will be further discussed later in the text associated with figures 6 and 7. Uni-axial compression excites both the shear and bulk stiffness peak and anti-peak. However, the width of the compression peak is different from that of the bulk or shear peak. The physical meaning of the width of a peak is unclear for the time being. It can be seen that to achieve a shear stiffness peak (or anti-peak) requires more negative k_1, when compared with the bulk stiffness peak. Since, in the meta-stable regime, the degree of instability increases with the amount of negative stiffness, the shear peak is more unstable than the bulk peak. These results provide guidance for experimental investigations. For example, the stiffness peak corresponding the uniaxial compression occurs at a lesser $|k_1|$ in the meta-stable regime. This indicates that it may be more feasible to observe the uniaxial stiffness anomaly, compared to the hydrostatic case. Moreover, anomalies in the bulk properties are observed prior to (at less-negative k_1 values during tuning) those in the shear, indicating that there is the potential for stable systems not subject to a band instability. This point is also suggested in a recent study from a continuum approach [13].

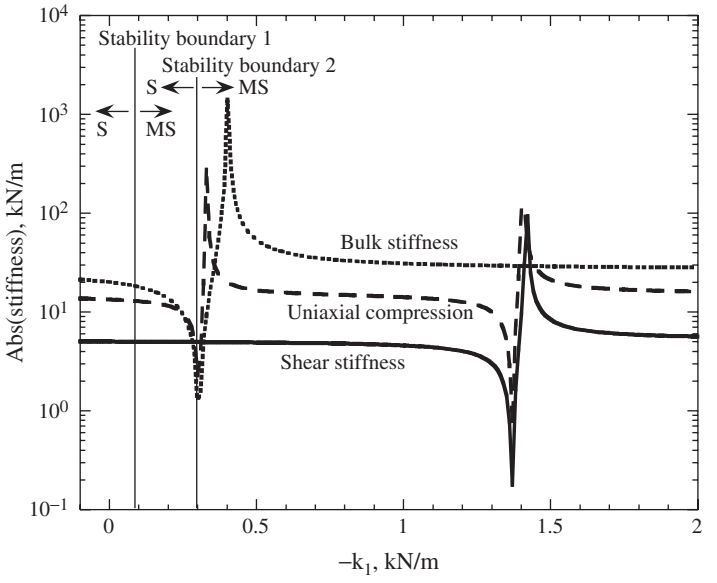

Figure 2. Overall bulk stiffness (K_b, dotted line), compressive stiffness (K_c, dashed line) and shear stiffness (K_s, solid line) *versus* k_1. When inertia (M_j) is greater than or equal to a critical value (10^{-6} kg, see section 3.2), the Lyapunov stability analysis predicts the stability boundary 2 for the system stability boundary, detailed in figures 6 and 7. The stability boundary 1 is obtained when $M_j = 10^{-12}$ kg or smaller, and the stability boundary 2 when $M_j = 10^{-6}$ kg or larger. The letters, S and MS, stand for stable and meta-stable, respectively.

Detailed information concerning the change of structural configuration with the reduction of k_1 under shear is shown in figures 3 and 4. The effective shear stiffness and area-change ratio versus the tuning parameter, k_1, are reported in figure 3. The area-change ratio for the outer triangle (not shown) is zero owing to simple shearing. It can be seen that there are two anti-peaks in the area-change ratio for the inner triangle, indicating minimal area changes at $k_1 \sim -1.31$ and -1.42 kN/m. They are due to change of orientation of the inner triangle. These two anti-peaks surround an area-change peak that corresponds to a maximum reduction of overall shear stiffness. This arrangement of peaks is also observed in the study of a hexagonal lattice structure with negative-stiffness components in [22]. Furthermore, the area-change anti-peak at $k_1 \sim -1.42$ kN/m is located very closely to the shear stiffness peak with a 0.007 kN/m difference, indicating that the cause of the extreme stiffness is due to the interplay of deformation modes between the inclusion and matrix [17]. However, this phenomenon is not observed in the case of hydrostatic compression [6].

The evolution of the geometrical configuration of the deformed structure with the order of decreasing k_1 is shown in figure 4. The inner triangle is indicated with thick solid lines, the outer triangle with thin solid lines and the linking elements dashed lines. The deformed geometry is normalized to the outermost boundary. Upon increasing the strength of the negative stiffness in the inner triangle, firstly, the shape of the inner triangle changes drastically from (a) to (b). Then a flip in the inner

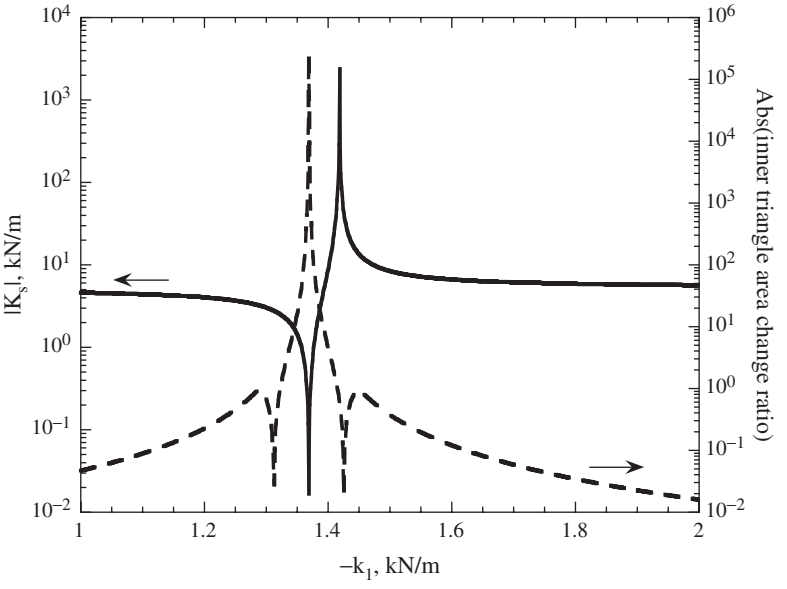

Figure 3. Overall shear stiffness (K_s) and area-change ratio *versus* k_1. The shear stiffness peak and anti-peak are located at $k_1 \sim -1.42$ and $k_1 \sim -1.37$ kN/m, respectively. The geometrical configurations of the structure around each of the peaks or anti-peaks for the area change ratio are shown in figure 4.

triangle occurs from (b) to (c). After that, the growth of the inner triangle in (d) and (e) is inevitable to maintain force balance by increasing the length of linking elements between the inner and outer triangle. A jump in switching orientation of the structure also occurs from (d) and (e). Continuing the increase of the magnitude of negative stiffness, the inner triangle shrinks with an orientation shown in (f). It appears as a mirror image of (c). Then, the inner triangle flips from (f) to (g). Finally, as shown in (h), the inner triangle roughly regains its original shape and size, but a different stretched orientation to that in (a), for $k_1 < -1.977$ kN/m. We remark that the shear loading condition is unchanged in all the figures. The changes of the geometrical configurations are due to the effects of negative stiffness. We also remark that the kinematical boundary conditions are satisfied in all the cases. Owing to the negative stiffness and equilibrium constraints, the inner triangle may exhibit unusual large deformation, according to the linear theory, as shown in (d) and (e). For the two-dimensional structure (as shown in figure 1), it is possible for the components to cross over one another when they are off-set into different planes. From a structural point of view, a generalization to the three dimensions is also possible if the components are made of the shell elements and empty space is provided so that components do not obstruct movements between them.

The results of overall damping calculations are shown in figure 5 with the following parameters fixed in the analysis. $\omega = 10$ Hz, $T_{\sigma 1} = 10^{-2}$ s, $T_{\varepsilon 1} = 10^{-4}$ s, $T_{\sigma 2} = 5 \times 10^{-2}$ s, $T_{\varepsilon 2} = 5 \times 10^{-4}$ s, $T_{\sigma 3} = 2 \times 10^{-2}$ s, $T_{\varepsilon 3} = 2 \times 10^{-4}$ s. The subscripts 1, 2 and 3 are in the same sense as those for the spring constants. We define r the ratio of T_σ to T_ε for each of the components in the structure, as in equation (7).

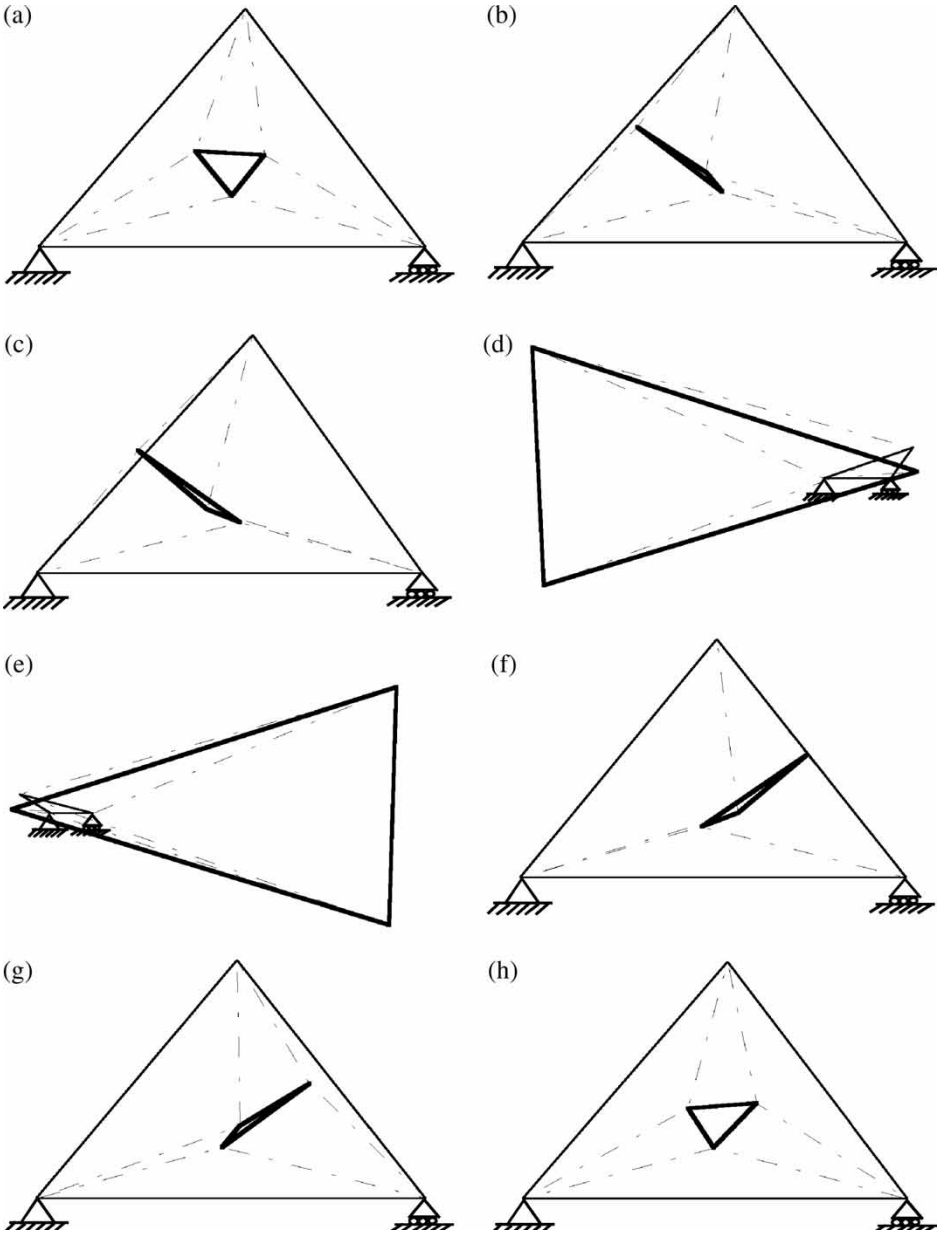

Figure 4. Evolution of structural geometry of the triangular structure with various k_1 under shear loading: (a) $k_1 = 0.205$, (b) $k_1 = -1.28$, (c) $k_1 = -1.301$, (d) $k_1 = -1.367$, (e) $k_1 = -1.371$, (f) $k_1 = -1.437$, (g) $k_1 = -1.462$ and (h) $k_1 = -1.977$. Stiffness is in units of kN/m. The inner triangle is composed of thick solid lines and the outer triangle of thin solid lines. Linking elements are denoted by dashed lines. Owing to the negative-stiffness and equilibrium constraints, the inner triangle may exhibit unusual large deformation, according to the linear theory, as shown in (d) and (e). Kinematical boundary conditions are satisfied in all the cases. The crossing over between components can be made possible when they are off set into different two-dimensional planes.

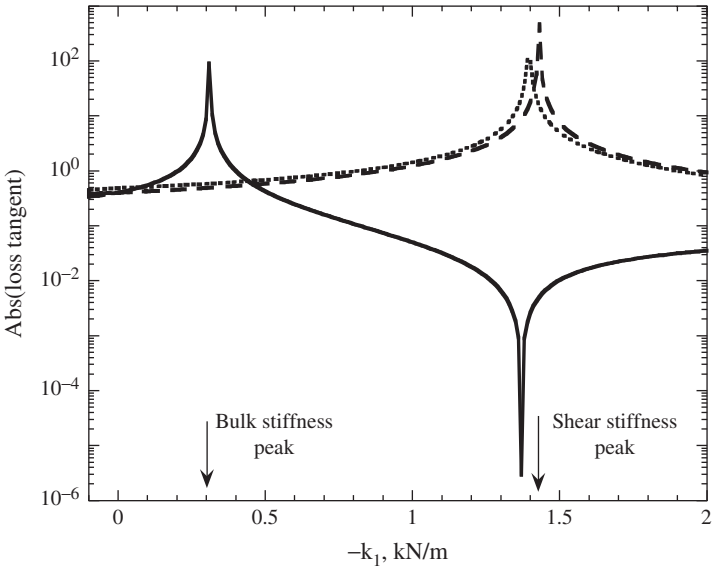

Figure 5. Anomalous damping peaks, calculated from equation (13). The bulk-damping peak (solid line) is at $k_1 \sim -0.3$ kN/m and the bulk anti-peak at $k_1 \sim -1.37$ kN/m. The shear-stiffness peak is at $k_1 \sim -1.42$ kN/m, obtained from figure 3. The damping peaks, dotted and dashed line, are at $k_1 \sim -1.395$ kN/m and $k_1 \sim -1.43$ kN/m, respectively.

When $r = 1$, the corresponding component is purely elastic. Our intention is to capture the low-frequency responses of the system with reasonable viscoelastic properties for the components. There are nine tan δ's from equation (13), and we plot only those exhibiting anomalies in terms of peaks or anti-peaks in the k_1 range of interest. We remark that our method of calculation gives all tan δ's for all deformation modes. The one-to-one correlation between a deformation mode and loss tangent can be sorted out by either performing eigenvector analysis, as in [17] for the 1-D cases, or identifying the simultaneous occurrence of a damping peak and stiffness anti-peak. Here, we adopt the latter. From figures 2 and 5, it can be seen that the damping peak around $k_1 \sim -0.3$ kN/m coincides with bulk stiffness anti-peak. Although a stiffness anti-peak indicates reduction in effective stiffness, the figure of merit, defined as the product of stiffness and damping, for the viscoelastic system may be high, owing to the higher magnitude of the damping peak. This has been shown for the 1-D cases [7]. The bulk damping anti-peak (at $k_1 \sim -1.37$ kN/m) is very close to the shear stiffness anti-peak, but pure shear loading will not excite it. The shear stiffness anti-peak is in relation to the damping peak at $k_1 \sim -1.395$ kN/m. The other damping peak at $k_1 \sim -1.43$ kN/m is related to other deformation mode. Comparing figures 3 and 5, it can be seen that the shear stiffness peak (at $k_1 \sim -1.42$ kN/m) is located between the two damping peaks. This implies that for certain loading conditions perfect alignment between stiffness and damping peaks, as observed in the 1-D systems, may not exist for systems with many degrees of freedom. The base-line magnitude of the overall damping varies with r, since it follows the damping of individual components.

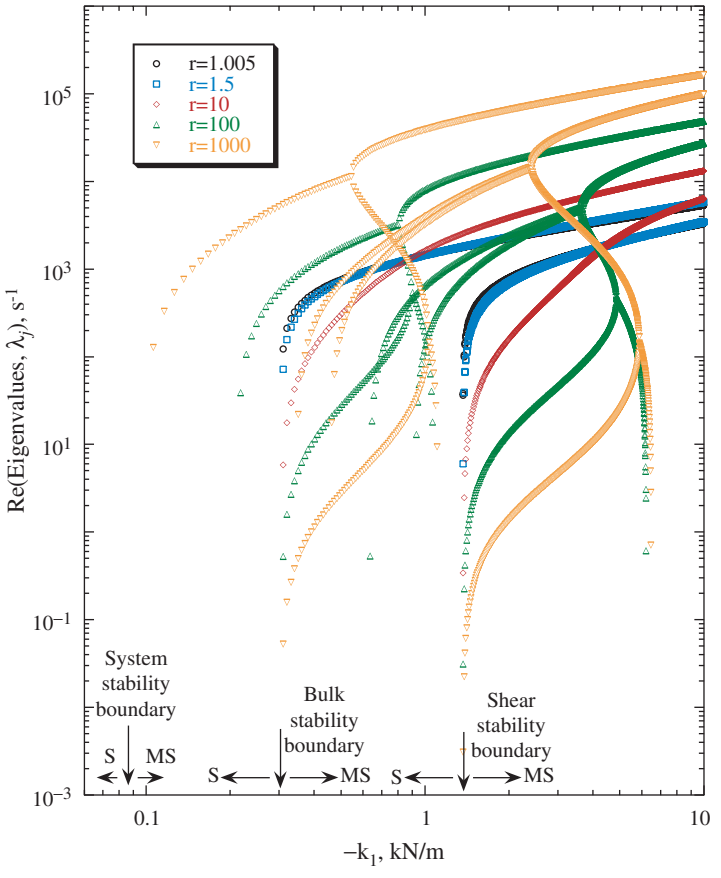

Figure 6. Dissipation-induced destabilization with $M_j = 10^{-6}$ kg, for all j. The symbol r denotes the strength of viscoelasticity of the components with $r = 1$ (black circles) for purely elastic materials. With increase of r (blue squares for $r = 1.5$; red diamonds for $r = 10$; green triangles for $r = 100$; orange downward triangles for $r = 1000$), the stability-losing eigenvalue curves move toward the less negative k_1 regime, indicating that the system can tolerate a lower amount of negative stiffness. For $10^3 < r < 10^6$, the system stability boundary remains the same at $k_1 \sim -0.09$ kN/m (not shown). For small r, the system and bulk stability boundaries coincide. The letters, S and MS, stand for stable and meta-stable, respectively.

3.2. *Results of stability analysis*

The stability losing eigenvalues (λ) are plotted against the tuning parameter k_1 in figures 6 and 7 for the cases of dissipation-induced destabilization (constant M_j) and inertia-induced stabilization (constant r), respectively. From the previous studies in the one-dimensional system [5, 7, 17], stability boundaries are independent of elemental damping and nodal masses. In the two-dimensional study [6], three stability boundaries are identified, corresponding to a system-related, bulk and shear mode. Moreover, stability boundaries are not influenced by damping inside components with $M_j = 10^{-12}$ kg for all j. It is worth noting that such small masses are used to ensure that the system is in quasi-static mode; consistent with our

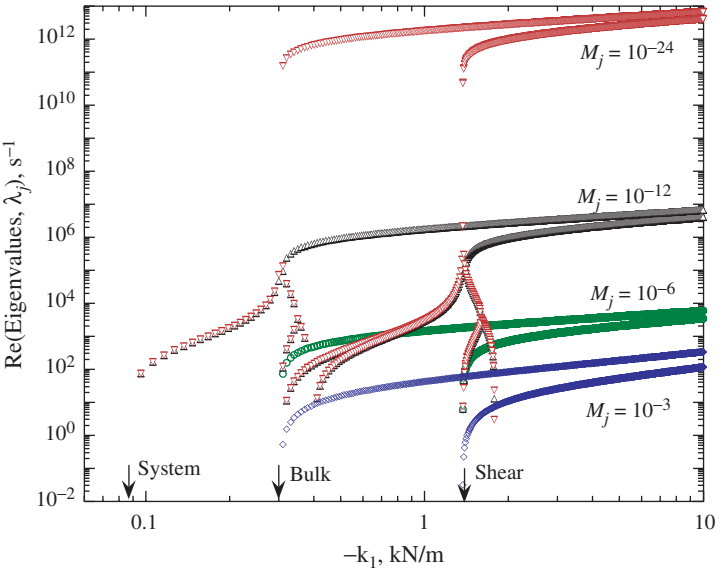

Figure 7. Inertia-induced stability with various M_j for fixed $r = 10$. With small masses $M_j \leq 10^{-12}$ kg for all j (black triangles and red downward triangles), the system stability boundary appears at $k_1 \sim -0.09$ kN/m. For $M_j \geq 10^{-6}$ kg for all j (green circles and blue diamonds), the system stability coincides with the stability boundary for the bulk mode at $k_1 \sim -0.3$ kN/m, indicating the structure can tolerate more negative stiffness while still Lyapunov stable. Eigenvalues with larger real part indicate high divergent rates.

interests in the low frequency dynamics of the system. In the present analysis, four cases are studied, corresponding to a chosen mass $M_j = 10^{-3}$, 10^{-6}, 10^{-12} or 10^{-24} kg for all j. In the case of $M_j = 10^{-6}$ kg, we observe that the structure is destabilized by the amount of damping inside its components in figure 6. For small elemental damping, $r \sim 1$, the structure stability depends on the bulk mode at $k_1 \sim -0.3$ kN/m (black circles). When $r = 1000$, stability-losing eigenvalues at $k_1 \sim -0.09$ kN/m (orange downward triangles) determine the overall stability of the whole system. For $10^3 < r < 10^6$, the system stability boundary stays with $k_1 \sim -0.09$ kN/m. The elemental damping also affects the magnitude of the eigenvalues, which determines the rate of divergence; eigenvalues with large real part indicate high divergent rates. To further discuss this issue, figure 7 shows the influences of inertia with a fixed $r = 10$. Following the trends of the curves of eigenvalues, it can be seen that when $M_j \geq 10^{-6}$ kg for all j, the system stability, coincident with the stability boundary for the bulk mode, is at $k_1 \sim -0.3$ kN/m. We determine that $M_j = 10^{-6}$ kg for all j is the critical inertia to maintain stability for the bulk damping peak. When $M_j \leq 10^{-12}$ kg for all j, the system is stable at $k_1 > -0.09$ kN/m. In the 1-D cases, the two parameters, mass and relaxation strength, do not affect the system stability, and the anomalous stiffness anti-peak coincides with the damping peak, the same as the system studied here for the bulk mode when $M_j \geq 10^{-6}$ kg. To the authors' knowledge, this is the first time that inertia-dependent stability is observed with such clarity in a dynamical system with or without the negative-stiffness influences.

To clarify, the critical inertia (10^{-6} kg) is determined by scanning the mass parameter in the inertia space, and observing changes in the stability eigenvalues *versus* the tuning parameter, k_1. This method can be readily applied to other dynamical systems, when one is interested in investigating the effect of a parameter on stability, in addition to the tuning parameter. An alternative way is to analytically perform stability analyses with respect to two or more tuning parameters in the framework of energy methods [23].

4. Conclusions

Anomalies in the effective stiffness and damping under hydrostatic, shear and uniaxial compression are observed for the two-dimensional nested triangular structure. Tracing the evolution of deformed geometry under shear loading, we observe that changes of the orientation of the inner triangle are responsible for the stiffness peaks and anti-peaks and, consequently, the effective damping peaks. The results of the Lyapunov stability analysis lead us to conclude that the system stability depends on inertia at the nodes and damping inside each of the standard linear solid components. When inertia is larger than or equal to a critical value (10^{-6} kg in the present case study), a stable loss-tangent peak can be achieved for the bulk mode in the two-dimensional system.

Acknowledgements

This research is funded by DOE, Office of Science, Office of Basic Energy Science. YCW acknowledges Los Alamos National Laboratory for the Director's post-doctoral fellowship. RSL is grateful for a grant, CMS-9896284, from NSF.

References

[1] R.S. Lakes, Phil. Mag. Lett. **81** 95 (2001).
[2] R.S. Lakes, T. Lee, A. Bersie, *et al*., Nature **410** 565 (2001).
[3] R.S. Lakes, Phys. Rev. Lett. **86** 2897 (2001).
[4] R.S. Lakes and W.J. Drugan, J. Mech. Phys. Solids **50** 979 (2002).
[5] Y.C. Wang and R.S. Lakes, Phil. Mag. **84** 3785 (2004).
[6] Y.-C. Wang, J.G. Swadener and R.S. Lakes, *Thin Solid Films* (2005), accepted for publication.
[7] Y.-C. Wang and R.S. Lakes, Appl. Phys. Lett. **84** 4451 (2004).
[8] G. Alberti and A. DeSimone, Proc. R. Soc. Lond. Ser. A **461** 79 (2005).
[9] R.S. Lakes, Science **235** 1038 (1987).
[10] R.S. Lakes, Adv. Mater. **5** 293 (1993).
[11] R.J. Knops and L.E. Payne, *Uniqueness Theorems in Linear Elasticity* (Springer, Berlin, 1971).

[12] R.J. Knops and E.W. Wilkes, in *Handbuck der physik,* VIa/1-4*,* edited by S. Flugge (Springer, Berlin, 1973), pp. 125–302.
[13] Y.-C. Wang and R.S. Lakes, J. Compos. Mater. **39** 1645 (2005).
[14] J.M.T. Thompson, Nature **296** 135 (1982).
[15] H. Ziegler, *Principles of Structural Stability* (Blaisdell Press, Waltham, MA, 1968).
[16] R. Bulatovic, C. R. Acad. Sci. Paris **324** 679 (1997).
[17] Y.-C. Wang and R.S. Lakes, Am. J. Phys. **72** 40 (2004).
[18] Y.-C. Wang and R.S. Lakes, Q. J. Appl. Math. **63** 34 (2005).
[19] K.-J. Bathe, *Finite Element Procedures in Engineering Analysis* (Prentice-Hall, Englewood Cliffs, NJ, 1982).
[20] R.D. Cook, D.S. Malkus and M.E. Plesha, *Concepts and Applications of Finite Element Analysis* (Wiley, New York, 1989).
[21] C. Zener, *Elasticity and Anelasticity of Metals* (University of Chicago Press, Chicago, 1948).
[22] Y.-C. Wang (2005), unpublished work.
[23] H. Leipholtz, *Stability of Elastic Systems* (Sijthoff & Noordhoff, Alphen aan den Rijn, The Netherlands, 1980).